Electronic Supplementary Material (ESI) for Nanoscale.

Supporting information for

Accelerated Size-focusing Light Activated Synthesis of Atomically Precise Fluorescent $Au_{22}(SR)_{16}$ Clusters

Parimah Aminfar, Travis Ferguson, Emily Steele, Emerson M. MacNeil, María Francisca Matus, Sami Malola, Hannu Häkkinen, Paul N. Duchesne, Hans-Peter Loock, and Kevin G. Stamplecoskie*

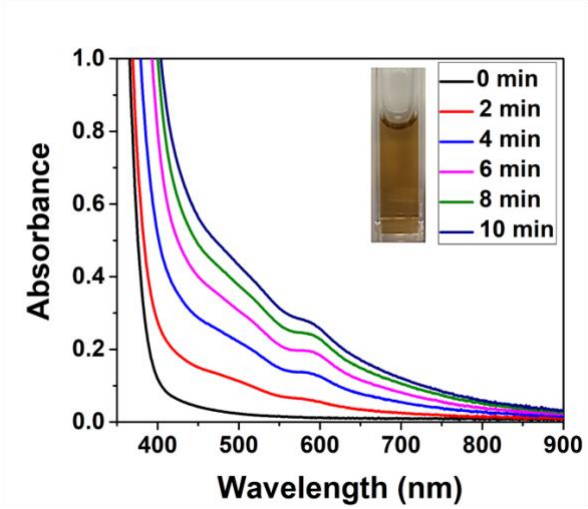

Fig S1. Absorbance spectra of $Au_x(Lys\text{-}Cys\text{-}Lys)_y$ mixture of nanoclusters formed during 10 minutes of irradiation with UVA light.

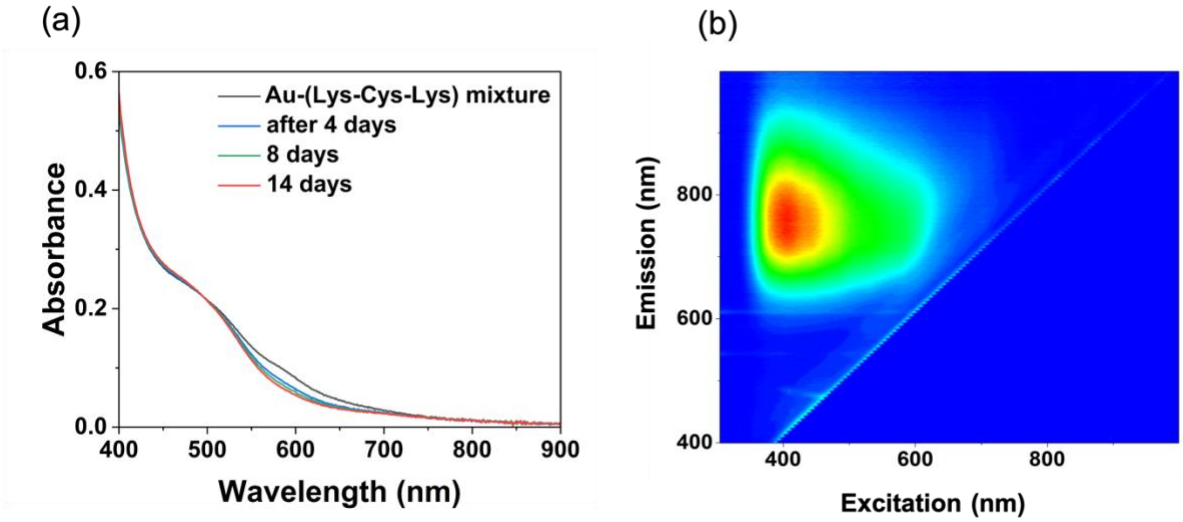

Fig S2. (a) Absorbance of $Au_x(Lys\text{-}Cys\text{-}Lys)_y$ mixture over the course of two weeks, and (b) fluorescence EEM of $Au_x(Lys\text{-}Cys\text{-}Lys)_y$ mixture after two weeks.

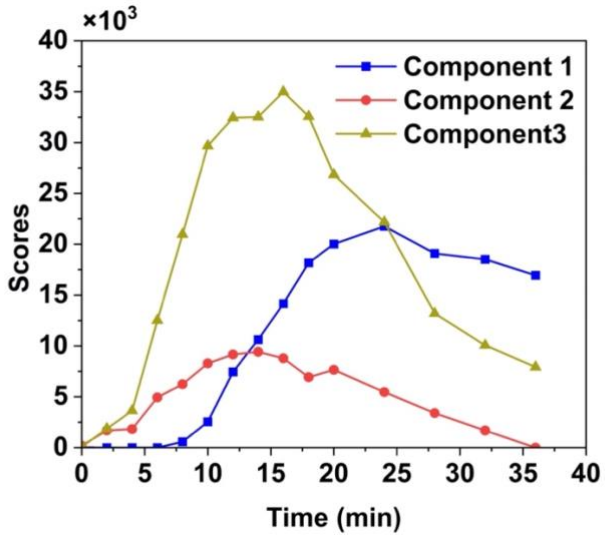

Fig S3. Score plot of the 3-component PARAFAC model calculated using drEEM toolbox for MATLAB after 30 min of UVA irradiation, showing the measure of each component during the synthesis.

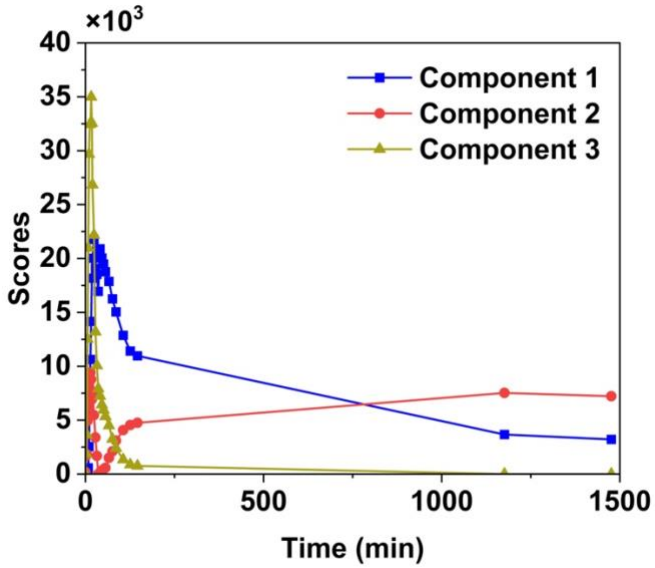

Fig S4. Score plot of the 3-component PARAFAC model calculated using drEEM toolbox for MATLAB after 30 min UVA irradiation followed by 24 h LED irradiation.

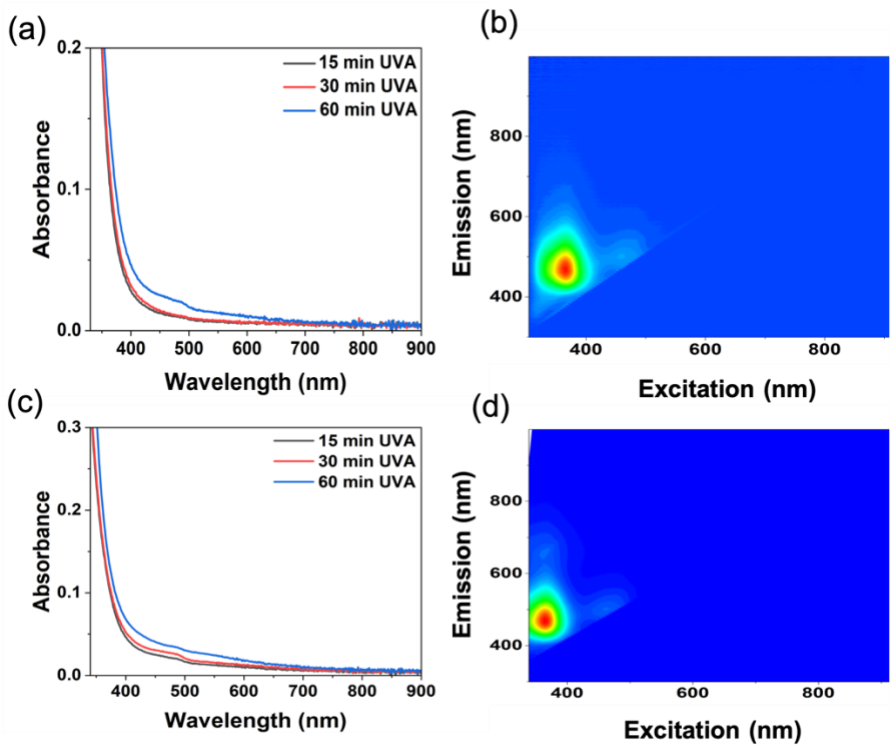

Fig S5. (a) and (b), absorbance and fluorescence EEM plot of Au-(Lys-Cys-Lys) species synthesized using 3 mM $HAuCl_4$ and 3 mM Omnirad-2959. (c) and (d), absorbance and fluorescence EEM plot of Au-(Lys-Cys-Lys) species synthesized using 3 mM $HAuCl_4$ and 9 mM Omnirad-2959.

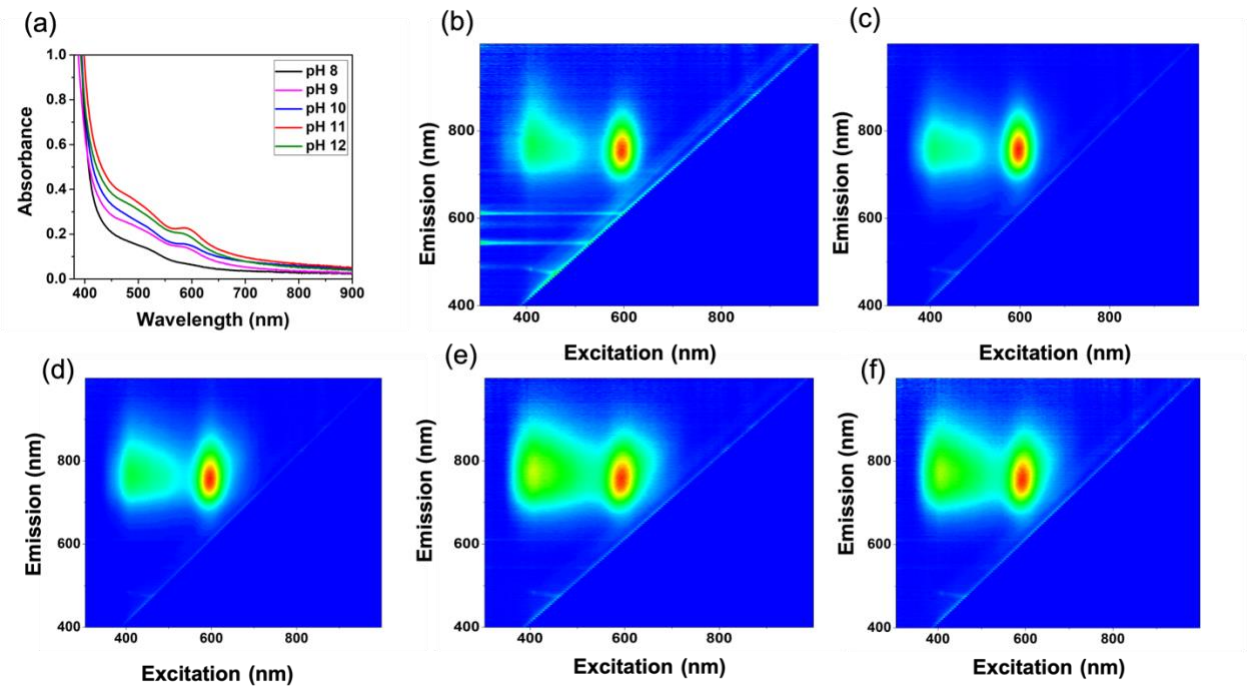

Fig S6. (a) Effect of pH on the (a) absorbance and (b-f) fluorescence EEM of $Au_x(Lys\text{-}Cys\text{-}Lys)_y$ clusters (from pH 8 to pH 12 respectively) after 12 min UVA irradiation.

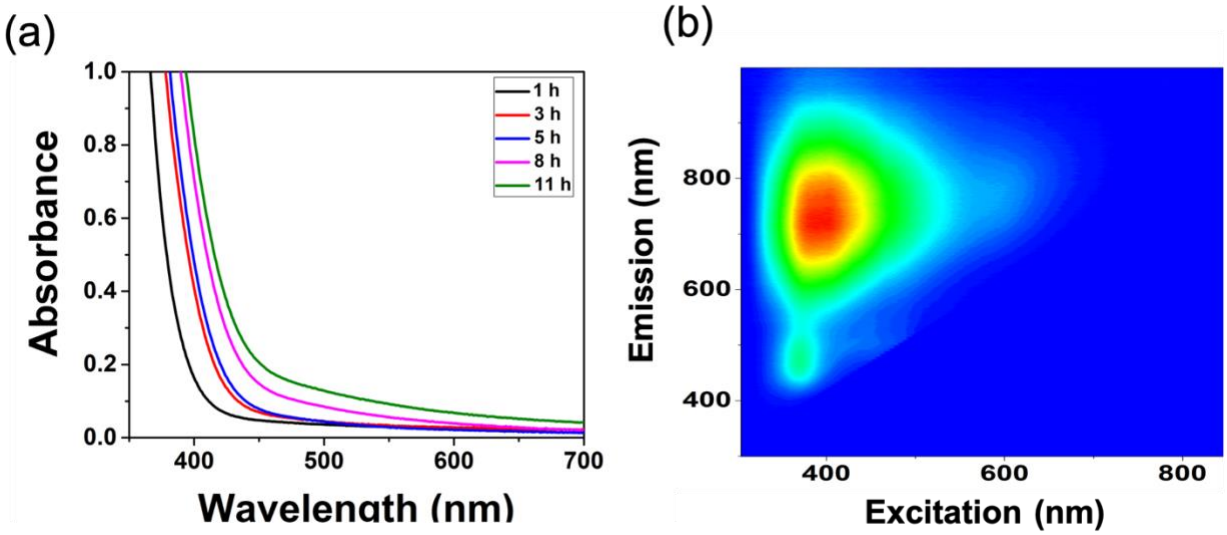

Fig S7. (a) absorbance and (b) fluorescence EEM plot of $Au_x(Lys\text{-}Cys\text{-}Lys)_y$ clusters synthesized using 340 nm laser instead of UVA lamps.

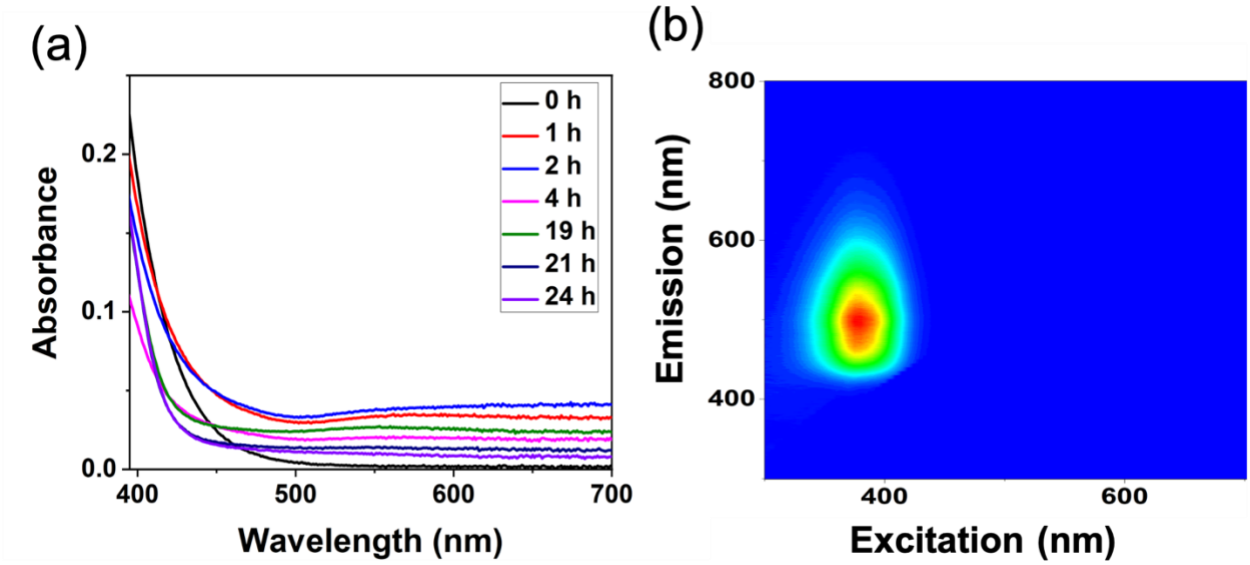

Fig S8. (a) absorbance and (b) fluorescence EEM plot of Au(I)-SR intermediates heated to 55°C for 24 h.

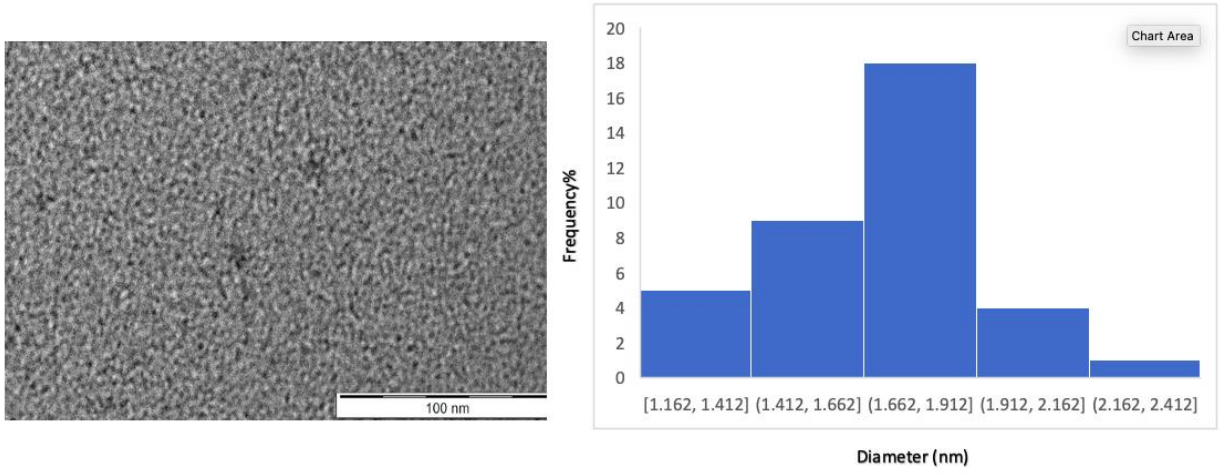

Fig S9. TEM image of Au_{22}(Lys-Cys-Lys)$_{16}$ clusters. The image background was removed before measuring the size of the particles that were significantly smaller than 2 nm.

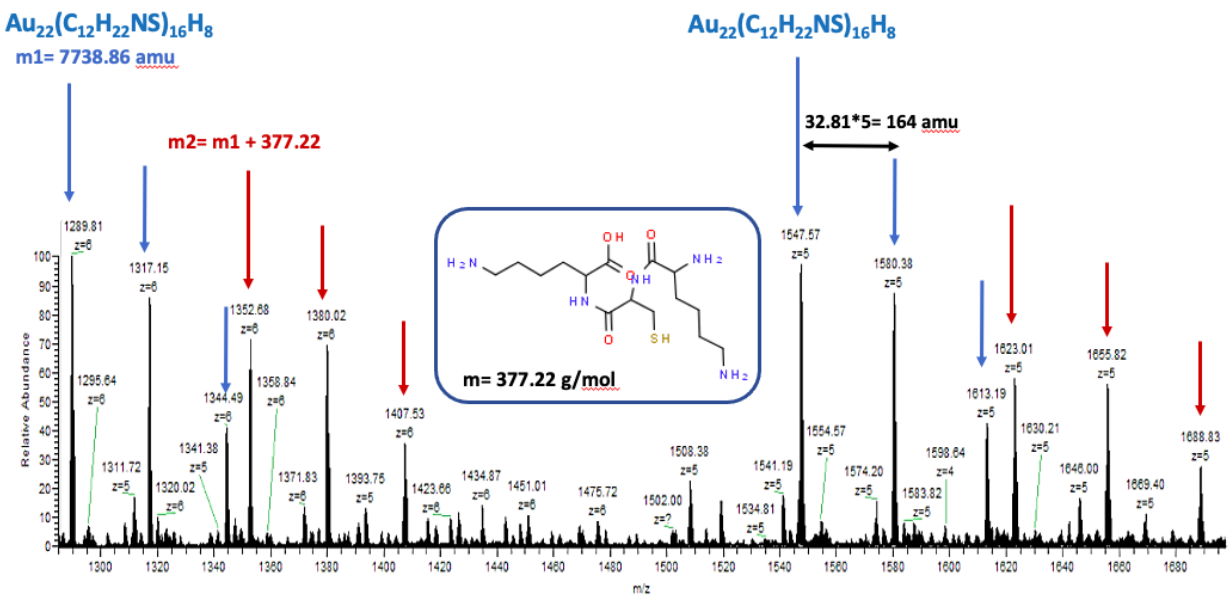

Fig S10. ESI-MS of $Au_x(Lys\text{-}Cys\text{-}Lys)_y$ mixture obtained using a spray voltage of 4 kV, sheath gas flow rate of 30, and capillary temperature of 100°C.

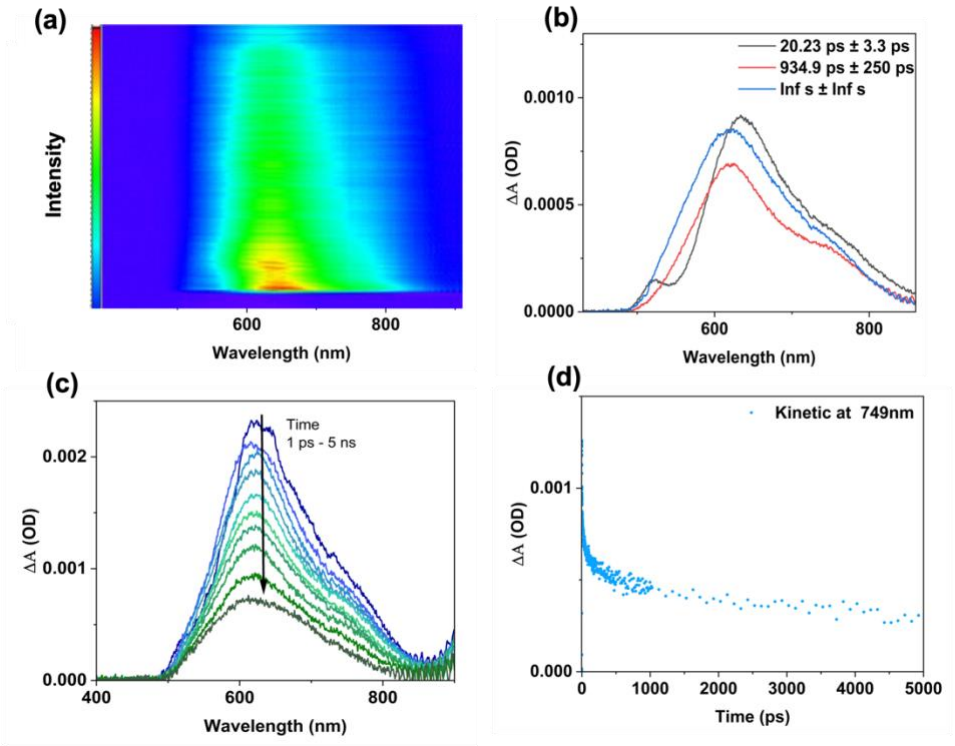

Fig S11. (a) Femtosecond transient absorption spectra of $Au_{22}(Lys\text{-}Cys\text{-}Lys)_{16}$ clusters excited at 340 nm, (b) three lifetime components, simulated from global analysis, that model the overall transient absorption spectra of $Au_{22}(Lys\text{-}Cys\text{-}Lys)_{16}$, (c) Overlaid transient absorption spectra of

Au_{22}(Lys-Cys-Lys)$_{16}$ clusters obtained at delay time of t=1 ps after excitation, and (d) femtosecond transient decay trace of Au_{22}(Lys-Cys-Lys)$_{16}$ clusters monitored at 749 nm.

Table S1. Amplitudes and lifetimes obtained from femtosecond transient absorption spectroscopy for Au_{22}(Lys-Cys-Lys)$_{16}$ nanoclusters, pumped at 340 nm and probed at 749 nm.

λ_{probe}	τ_1 (ps)	A_1	τ_2 (ps)	A_2	τ_3 (ps)	A_3
749 nm	1.01 ± 0.08	2.66 x 10^{-4}	29.54 ± 1.94	2.62 x 10^{-4}	1042.83 ± 66.45	2.99 x 10^{-4}

To replicate the thermal disorder observed during data collection, the experimentally determined Debye-Waller factor of 0.0029 Å^2 (Table 2) was used when simulating the EXAFS spectrum of the DFT-calculated structure. By using the same Debye-Waller factor, this corrects for thermal effects, such as amplitude suppression and peak broadening. The corresponding amplitude reduction factor (S_0^2) of 0.9 was obtained by fitting the Au foil reference and was fixed during EXAFS fitting. The amplitude reduction factor accounts for multiple electron excitations and scales the spectrum accordingly.[1] Theoretical scattering paths of the DFT-predicted $Au_{22}(L)_{16}$ structure were obtained using FEFF8 computational software and used in fitting the experimental EXAFS data. The k-range used for EXAFS fitting was 1.0 to 9.0 Å^{-1}.

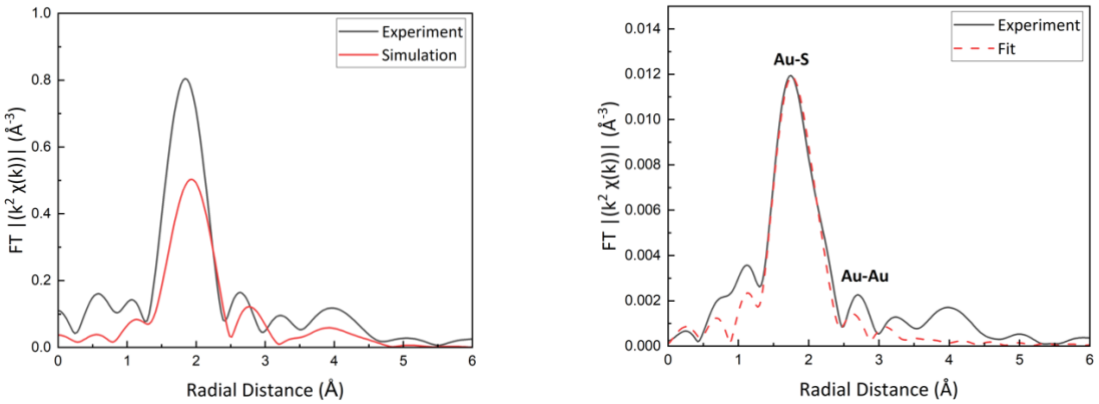

Fig S12. a) Au L_3-edge FT-EXAFS of the DFT-predicted $Au_{22}(L)_{16}$ cluster (red line) and the experimental Au_{22}(Lys-Cys-Lys)$_{16}$ data (black line), and b) experimental Au L_3-edge FT-EXAFS spectrum (black line) and the best fit based on the Au-S scattering path from the predicted model (dotted red line).

Table S2. Au L_3-edge EXAFS fitting results of Au_{22}(Lys-Cys-Lys)$_{16}$

Path	CN	R (Å)	σ^2 (Å^2)	E0 Shift (eV)
Au-S	2.19 ± 0.30	2.29 ± 0.01	0.0029 ± 0.0017	-1.54 ± 1.29

The red arrows in Fig. S13 and S14 indicate the absorbance features associated with ABDA. ABDA undergoes oxidation to form endoperoxide $ABDAO_2$ when $^1O_2$ is generated by clusters, leading to loss in absorbance of ABDA at 350 – 400 nm. The positive control used in this study was methylene blue (MB) which is commonly used for the photochemical generation of $^1O_2$ (with QY of 0.52). Using equimolar concentrations of ABDA in water, two solutions were prepared. The first solution contained 50 µL of ABDA stock solution (0.15 mg/ml) which was added to the clusters with a total solution volume of 2.6 ml, where the absorbance of the clusters and the probe were set to 0.2 at 520 nm (excitation wavelength). To the second solution, 50 µL of ABDA stock solution was added to a 2.6 ml MB solution, where the absorbance of the MB and the probe were matched at 520 nm. Using 520 nm LED light, the solutions were irradiated in 5-minute intervals up to 30 minutes and absorbance spectra were acquired at each interval.

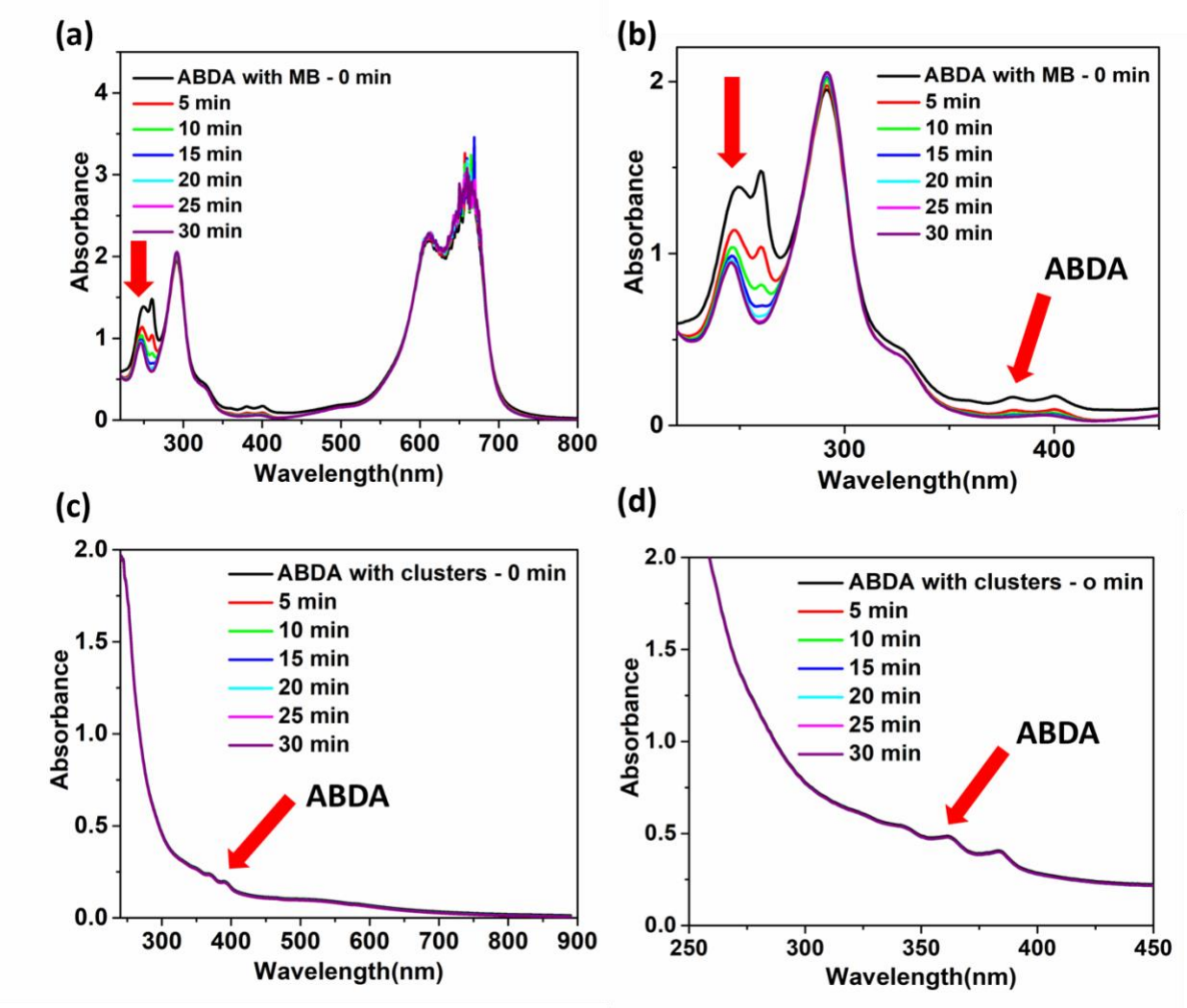

Fig S13. Absorbance spectra of (a) MB (control) and (c) Au_{22}(Lys-Cys-Lys)$_{16}$ clusters in ABDA aqueous solution. (b) and (d) show the zoomed spectrum for (a) and (b), respectively. The absorbance of the clusters and ABDA were set to 0.1 at 520 nm. No absorbance decrease was observed with Au_{22}(Lys-Cys-Lys)$_{16}$ clusters added to the ABDA solution and the solution was

irradiated with 520 nm LEDs, indicating singlet oxygen cannot be generated from their excited state.

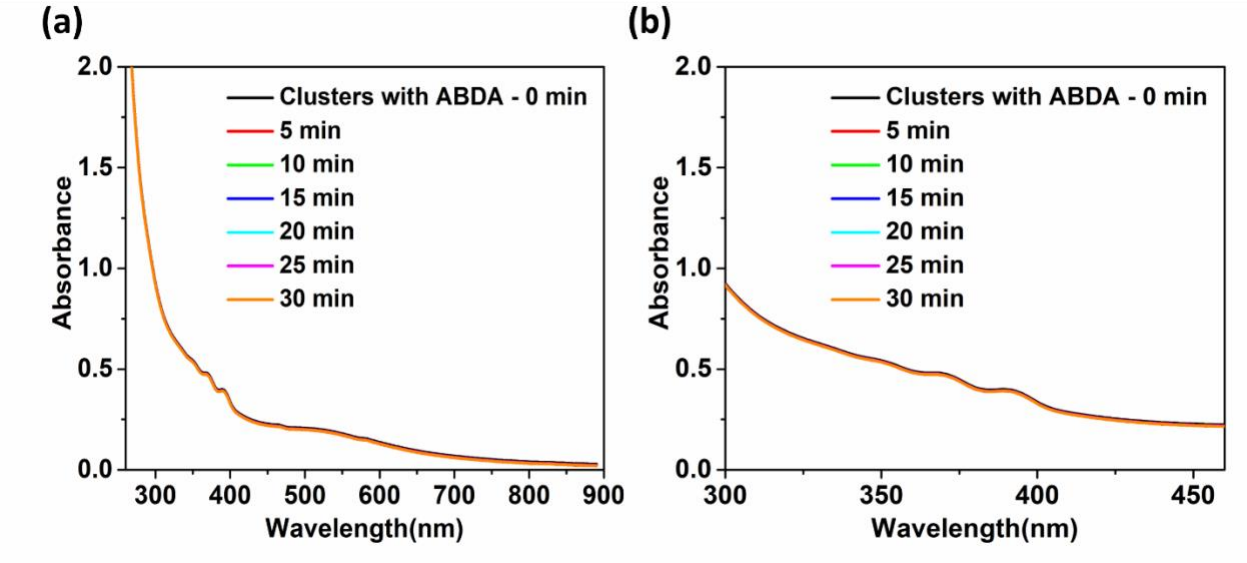

Fig S14. Absorbance spectra of (a) MB (control) and (c) Au_{22}(Lys-Cys-Lys)$_{16}$ clusters in ABDA aqueous solution (replicate experiment). The absorbance of the clusters and ABDA were set to 0.2 at 520 nm this time. No absorbance decrease was observed with Au_{22}(Lys-Cys-Lys)$_{16}$ clusters added to the ABDA solution and the solution was irradiated with 520 nm LEDs, indicating singlet oxygen cannot be generated from their excited state.

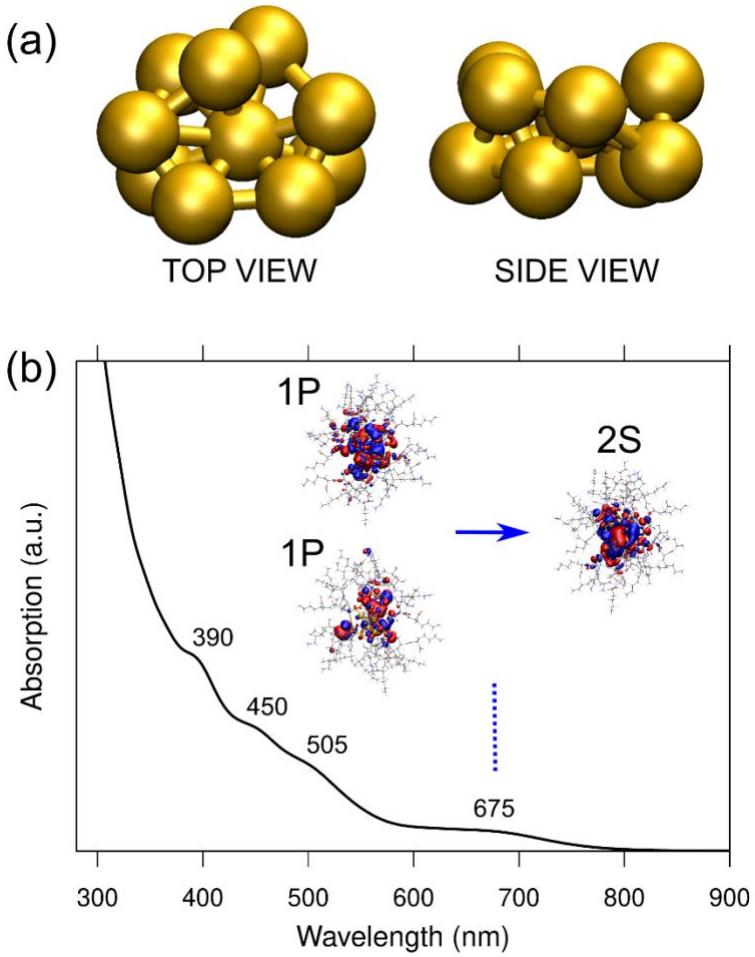

Fig S15. a) top view and side view of the metal core of the calculated model structure. b) calculated optical absorption spectrum of the neutral $Au_{22}(Lys\text{-}Cys\text{-}Lys)_{16}$ model cluster. Four absorption features are identified and labeled, from which the first at 675 nm originates from transitions between 1P and 2S states visualized in the figure.

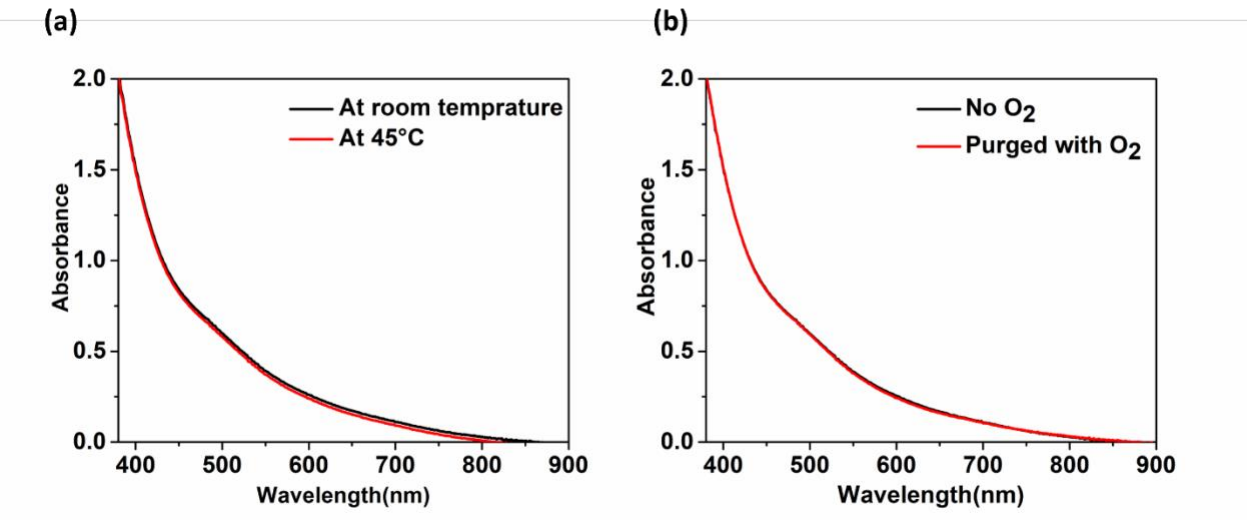

Fig S16. Absorbance spectra of Au_{22}(Lys-Cys-Lys)$_{16}$ clusters before and after (a) heating at 45°C and (b) O_2 treatment.

Molecular dynamics (MD) simulations of Au_{22}(Lys-Cys-Lys)$_{16}$ cluster

Classical MD simulations were carried out with GROMACS 2022[2] using a previously published force field for thiolate-protected gold nanoclusters.[3] First, the partial atomic charges of the Lys-Cys-Lys ligands were obtained using a Au_2(Lys-Cys-Lys)$_2$ model[3, 4] following the two-stage RESP fitting procedure recommended for Amber[5] using Ambertools16.[6] The GROMACS topologies for the Lys-cys-Lys ligands were generated with ACPYPE code[7] and added to the force field.

The DFT-based model structure of Au_{22}(Lys-Cys-Lys)$_{16}$ cluster was placed in the center of a cubical box filled with TIP3P water molecules[8] and neutralized with counterions (0.15 M NaCl).[9] Energy minimization was carried out using the steepest descent method followed by a short equilibration consisting of 10 ns NVT (constant number of particles, volume, and temperature) at 300 K and then 10 ns NPT (constant number of particles, pressure, and temperature) at 300 K and 1 bar pressure using the V-rescale thermostat and Berendsen barostat.[10] Then, 500 ns of production MD was performed using a 2.0 fs timestep (leapfrog Verlet integrator) by keeping the temperature at 300 K with the V-rescale thermostat[11] and pressure at 1 bar using Parinello-Rahman barostat[12] with a period of 2.0 ps. The van der Waals interactions were modeled with Lennard–Jones potentials truncated at 1.0 nm, while electrostatic interactions were modeled with the particle-mesh Ewald (PME) method[13] with a cutoff of 1.0 nm and 0.12 nm grid spacing. The bond lengths to hydrogens in the nanocluster were constrained with the LINCS algorithm for improved performance.[14]

The MD trajectory was visualized in VMD[15] and the Root-mean-square deviation (RMSD) and radius of gyration (Rg) analyses as a function of simulated time were carried out using the utility toolkits of GROMACS (gmx rms and gmx gyrate, respectively).

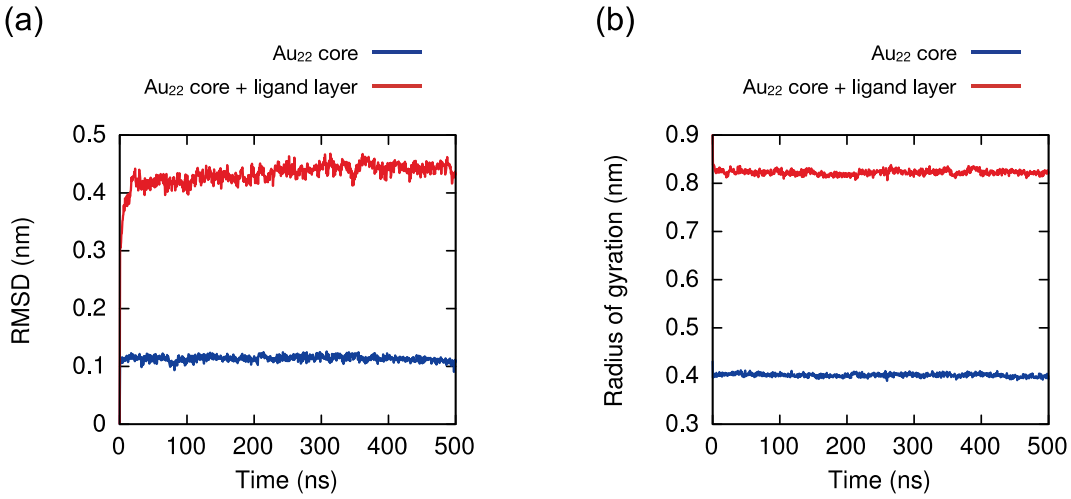

Fig S17. Root-mean-square deviation (RMSD) of a) atomic positions and b) radius of gyration (Rg) of the DFT-based model structure of Au_{22}(Lys-Cys-Lys)$_{16}$ cluster as a function of simulation time for molecular dynamics. RMSD: 0.11 ± 0.005 nm and 0.43 ± 0.018 nm for metal core and metal core + ligand layer, respectively. Rg values are 0.40 ± 0.003 nm and 0.82 ± 0.005 nm for metal core and metal core + ligand layer, respectively.

References

1. M. Roy, S. J. Gurman and G. E. v. Dorssen, *Journal De Physique Iv*, 1997, **7**.
2. M. J. Abraham, T. Murtola, R. Schulz, S. Páll, J. C. Smith, B. Hess and E. Lindahl, *SoftwareX*, 2015, **1-2**, 19-25.
3. E. Pohjolainen, X. Chen, S. Malola, G. Groenhof and H. Häkkinen, *J Chem Theory Comput*, 2016, **12**, 1342-1350.
4. M. F. Matus, S. Malola and H. Häkkinen, *ACS Nanoscience Au*, 2021, **1**, 47 - 60.
5. C. I. Bayly, P. Cieplak, W. Cornell and P. A. Kollman, *The Journal of Physical Chemistry*, 1993, **97**, 10269-10280.
6. D. A. Case, Betz, R., Cerutti, D., Cheatham, T.E., Darden, T., Duke, R.E., Giese, T., Gohlke, H., Goetz, A., and Homeyer, N, 2016, AMBER 16. 2016. San Fr.
7. A. W. Sousa da Silva and W. F. Vranken, *BMC Research Notes*, 2012, **5**, 367.
8. W. L. Jorgensen, J. Chandrasekhar, J. D. Madura, R. W. Impey and M. L. Klein, *The Journal of Chemical Physics*, 1983, **79**, 926-935.
9. A. A. Chen and R. V. Pappu, *J Phys Chem B*, 2007, **111**, 11884-11887.
10. H. J. C. Berendsen, J. P. M. Postma, W. F. van Gunsteren, A. DiNola and J. R. Haak, *The Journal of Chemical Physics*, 1984, **81**, 3684-3690.

11. G. Bussi and M. Parrinello, *Computer Physics Communications*, 2008, **179**, 26-29.
12. M. Parrinello and A. Rahman, *Journal of Applied Physics*, 1981, **52**, 7182-7190.
13. T. Darden, D. York and L. Pedersen, *The Journal of Chemical Physics*, 1993, **98**, 10089-10092.
14. B. Hess, H. Bekker, H. J. C. Berendsen and J. G. E. M. Fraaije, *Journal of Computational Chemistry*, 1997, **18**, 1463-1472.
15. W. Humphrey, A. Dalke and K. Schulten, *Journal of Molecular Graphics*, 1996, **14**, 33-38.